# High-Performance Stand-Alone Photovoltaic Generation System

Rong-Jong Wai, *Senior Member, IEEE*, Wen-Hung Wang, and Chung-You Lin

***Abstract*—This study develops a high-performance stand-alone photovoltaic (PV) generation system. To make the PV generation system more flexible and expandable, the backstage power circuit is composed of a high step-up converter and a pulsewidth-modulation (PWM) inverter. In the dc–dc power conversion, the high step-up converter is introduced to improve the conversion efficiency in conventional boost converters to allow the parallel operation of low-voltage PV arrays, and to decouple and simplify the control design of the PWM inverter. Moreover, an adaptive total sliding-mode control system is designed for the voltage control of the PWM inverter to maintain a sinusoidal output voltage with lower total harmonic distortion and less variation under various output loads. In addition, an active sun tracking scheme without any light sensors is investigated to make the PV modules face the sun directly for capturing the maximum irradiation and promoting system efficiency. Experimental results are given to verify the validity and reliability of the high step-up converter, the PWM inverter control, and the active sun tracker for the high-performance stand-alone PV generation system.**

***Index Terms*—Active sun tracking scheme, adaptive total sliding-mode control (ATSMC), high step-up converter, photovoltaic (PV) generation system, pulsewidth-modulation (PWM) inverter.**

## I. Introduction

In the past century, global surface temperatures have increased at a rate near 0.6 °C/century because of global warming caused by effluent gas emissions and increases in $CO_2$ [1], [2] levels in the atmosphere. The problems with energy supply and use are related not only to global warming but also to such environmental concerns as air pollution, acid precipitation, ozone depletion, forest destruction, and radioactive substance emissions. To prevent these effects, some potential solutions have evolved including energy conservation through improved energy efficiency, a reduction in fossil fuel use and an increase in environmentally friendly energy supplies. Recently, energy generated from clean, efficient and environmentally-friendly sources has become one of the major challenges for engineers and scientists. Among them, the photovoltaic (PV) generation system has received great attention in research because it appears to be one of the possible solutions to the environmental problem [3]–[7].

Recently, dc–dc converters with high voltage gain have become usually required in many industrial applications such as the front-end stage for clean-energy sources, the dc back-up energy system for uninterruptible power supply, high-intensity discharge lamps for automobile headlamps, and telecommunication industry applications [8]–[11]. The conventional boost converters cannot provide such a high dc voltage gain, even for an extreme duty cycle. It also may result in serious reverse-recovery problem and increase the rating of all devices. As a result, the conversion efficiency is degraded and the electromagnetic interference problem is severe under this situation [12]. To increase the conversion efficiency and voltage gain, many modified step-up converter topologies have been investigated in the past decades [13]–[17]. Although voltage-clamped techniques are manipulated in the converter design to overcome the severe reverse-recovery problem of the output diode in high-level voltage applications, there still exist overlarge switch voltage stresses and the voltage gain is limited by the turn-on time of the auxiliary switch [13], [14]. Wai and Duan [17] investigated a novel coupled-inductor converter strategy to increase the voltage gain of a conventional boost converter with a single inductor, and deal with the problem of the leakage inductor and demagnetization of the transformer in a conventional coupled-inductor-based converter. In this paper, the high step-up converter topology in [17] is introduced to boost and stabilize the output dc voltage of PV modules for the utilization of a dc–ac inverter.

Developments in microelectronics and power devices have caused the widespread application of pulsewidth-modulation (PWM) inverters in industries. The basic mechanism of a PWM inverter is to convert the dc voltage to a sinusoidal ac output through the inverter-$LC$ filter blocks. The performance is evaluated by the total harmonic distortion (THD), the transient response, and the efficiency. Thus, much attention has been paid to the closed-loop regulation of PWM inverters to achieve good dynamic response under different types of loads in the past decade, e.g., linear control [18], observer for grid current control [19], Lyapunov-based control [20], sliding-mode control (SMC) [21], etc. Variable structure control with sliding mode, or SMC, is one of the effective nonlinear robust control approaches since it provides system dynamics with an invariance property to uncertainties once the system dynamics are controlled in the sliding mode [20]–[23]. The insensitivity of the controlled system to uncertainties exists in the sliding mode, but not during the reaching phase, i.e., the system dynamic in the reaching phase is still influenced by uncertainties. Recently,

Manuscript received February 23, 2006; revised September 12, 2007. This work was supported in part by the National Science Council of Taiwan, R.O.C., through Grant 95-2221-E-155-070-MY3.

R.-J. Wai and C.-Y. Lin are with the Department of Electrical Engineering, Yuan Ze University, Chung Li 320, Taiwan, R.O.C. (e-mail: rjwai@saturn.yzu.edu.tw).

W.-H. Wang was with the Department of Electrical Engineering, Yuan Ze University, Chung Li 320, Taiwan, R.O.C. He is now with the Ministry of National Defense, Taipei 100, Taiwan.

Digital Object Identifier 10.1109/TIE.2007.896049

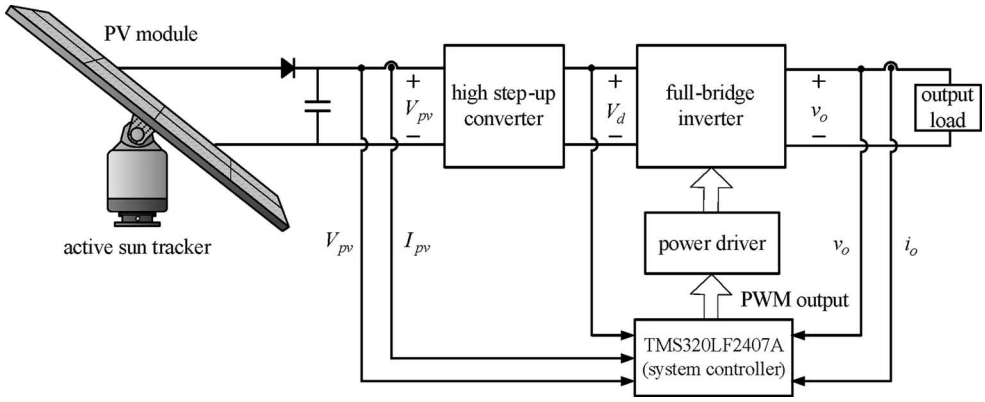


Fig. 1. Configuration of a high-performance stand-alone PV generation system.

some researchers have adopted the idea of total SMC (TSMC) to get a sliding motion through the entire state trajectory [24]–[26], i.e., no reaching phase exists in the control process, so that the controlled system through the whole control process is not influenced by uncertainties. This paper attempts to extend an adaptive TSMC (ATSMC) from [25] to the voltage control of a PWM inverter. Up to now, this is the first time that the application of TSMC to the power electronics control is investigated.

In general, the output power of a PV module is substantially changed according to different irradiations. For example, in Taiwan, the direction with the maximum average irradiations during the year is South, and the corresponding angle of inclination is 23.5° so that many PV modules are installed in this posture. However, the maximum irradiations cannot be captured persistently in this way such that the performance of the PV generation system cannot be improved effectively. Recently, many researchers have made efforts in sun tracking investigations [27]–[30]. The conventional sun tracking strategies equip light sensors on the terminals of PV plates. When the feedback signals from light sensors are equal, it means that the PV plate faces the sun and has the maximum irradiation at the corresponding position. Unfortunately, the initial proofreading and correcting of light sensors are time consuming and the device properties are easily varied under different operational conditions. In order to overcome the aforementioned drawbacks, this paper investigates an active sun tracking scheme without light sensors via the property of the open-circuit voltage of PV modules proportional to the corresponding irradiation to follow the trail of the sun.

The topic of this paper focuses on the development of a high-performance stand-alone PV generation system. It contains three main contents including a high step-up converter, a PWM inverter with ATSMC, and an active sun tracking scheme. First, the active sun-tracking scheme is designed to capture maximum irradiation and powers. Then, the high step-up converter is implemented for converting the captured power from the active sun-tracking scheme to form a stable dc voltage source. In addition, the PWM inverter with ATSMC transfers this dc voltage source from the high step-up converter into an ac voltage source for stand-alone utilization. This paper is organized into seven sections. Following the introduction, the entire configuration and key components of a high-performance stand-alone PV generation system are described briefly in Section II. It is a stand-alone PV application, where voltage control is needed. Moreover, the system architecture and operational principle of a high step-up converter are illustrated in Section III. In Section IV, the dynamic average model of a PWM inverter scheme is introduced to simplify the subsequent development of an ATSMC scheme for ensuring the corresponding output power quality. In addition, an active sun tracking scheme is further proposed to enhance the system performance in Section V. In Section VI, experimental results are performed to demonstrate the efficiency and applicability of the developed methodologies for a PV generation system. Finally, some conclusions are drawn in Section VII.

## II. System Description

In this paper, the configuration of a high-performance stand-alone PV generation system is depicted in Fig. 1. The system is mainly composed of a PV module, an active sun tracker, a high step-up converter, a full-bridge inverter, a system controller, and an output load. The identified problems in conventional PV generation systems and the proposed solutions in this paper are expressed in detail as follows. Due to the PV effect, the voltage of a PV plate is not very high. However, the PV array with a higher output voltage is difficult to fabricate and it may fail when any single PV plate is inactive. Besides, the corresponding output voltage $(V_{\rm pv})$ is varied easily with respect to the variation of loads. To satisfy the requirement of high-voltage demand, a high-efficiency dc–dc converter with high voltage gain is needed as one of the essential mechanisms in the high-performance stand-alone PV generation system. In this paper, a high step-up converter [17] is implemented to reduce the series-connected numbers of PV plates, to maintain a constant dc bus voltage $(V_{\rm d})$ for the inverter utilization, and to decouple and simplify the control design of a dc–ac inverter.

A unipolar PWM full-bridge inverter with four power semiconductors and a low-pass filter is regarded as the dc–ac power conversion circuit to meet the requirement of an ac power source. Since the PWM inverter dominates the performance in converting the dc voltage source to an ac voltage source,

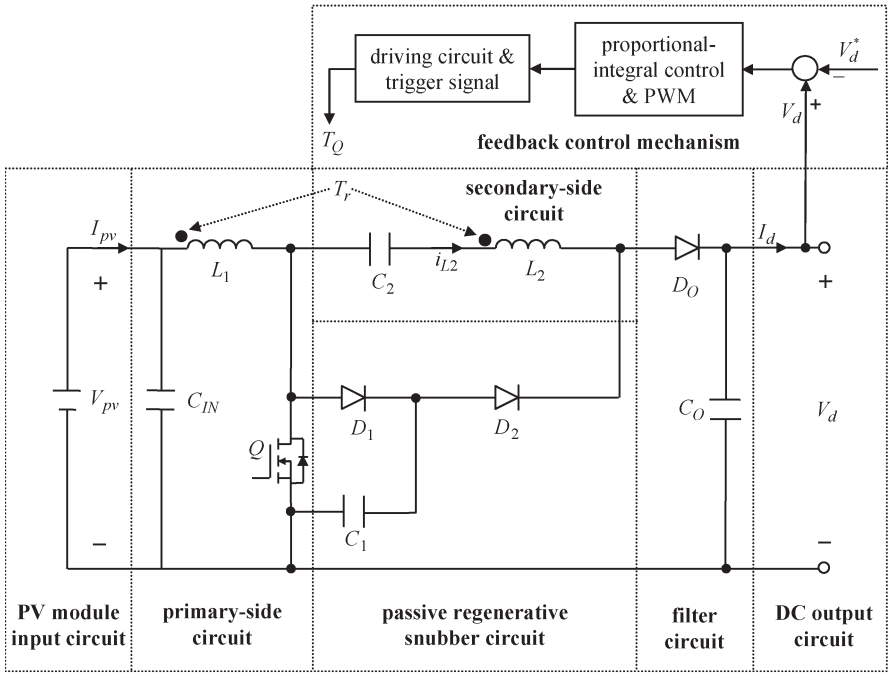


Fig. 2. Architecture of high step-up converter.

the quality of the ac output waveform of the PV generation system is highly dependent on the performance of the PWM inverter. Thus, an ATSMC system [25] is introduced by way of switching four power semiconductors in this inverter to maintain a sinusoidal output voltage $(\nu_{\rm o})$ with lower THD and less variation under various output loads. While reviewing previous works in published literatures [20]–[26], no related research reports were found that investigate the application of the ATSMC system in power electronics control.

Generally speaking, the output power of a PV module is substantially changed according to different irradiations. To further enhance the performance of the stand-alone PV generation system, an active sun tracker actuated by a synchronous motor is investigated on the basis of the open-circuit voltage of the PV modules. This keeps the PV plate facing the sun to improve the generation efficiency of the fixed-installation PV module, and to save the cost associated with the conventional sun tracker with light sensors. This way, it is not necessary to modify the original circuit framework of the PV generation system because of the simple requirement of the open-circuit voltage of PV modules in the active sun tracking scheme.

In this paper, the PWM inverter control and the active sun tracking scheme are carried out using Turbo C language written in a system controller, i.e., a digital signal processor (DSP) development module. This development module has a Texas Instruments TMS320LF2407A central processing unit with an evaluation module, 16-channel 10-bit analog-to-digital, 4-channel 12-bit digital-to-analog converters and programmable input–output (I/O) ports. The central processing unit has a 40MIPS 16-bit fixed point DSP core, 16 PWM channels, four general purpose timers and two encoder channels. The detailed functions of the main components in the PV generation system are described in the following sections.

## III. High Step-Up Converter

The architecture of a high step-up converter introduced in [17] is depicted in Fig. 2, where it contains seven parts including a PV module input circuit, a primary-side circuit, a secondary-side circuit, a passive regenerative snubber circuit, a filter circuit, a dc output circuit, and a feedback control mechanism. In this strategy, a coupled inductor with a low-voltage-rated switch is used for raising the voltage gain whether the switch is turned on or off. Moreover, a passive regenerative snubber is utilized for absorbing the energy of stray inductance so that the switch duty cycle can be operated under a wide range, and the related voltage gain is higher than other coupled-inductor-based converters. In addition, all devices in this scheme also have voltage-clamped properties and their voltage stresses are relatively smaller than the output voltage. Thus, it can select low-voltage low-conduction-loss devices, and there are no reverse-recovery currents within the diodes in this circuit. Furthermore, the closed-loop control methodology is utilized to overcome the voltage drift problem of the power source under the load variations. As a result, this converter topology can increase the voltage gain of a conventional boost converter with a single inductor, and deal with the problem of the leakage inductor and demagnetization of the transformer for a coupled-inductor-based converter.

The major symbol representations are summarized as follows. $V_{\rm pv}$ and $I_{\rm pv}$ denote dc input voltage and current, and $C_{\rm IN}$ is an input filter capacitor in the PV module input circuit. $L_1$ and $L_2$ represent individual inductors in the primary and secondary sides of the coupled inductor $(T_{\rm r})$, respectively. $Q$ is a switch in the primary-side circuit; $V_{\rm d}^*$ and $T_Q$ are the output voltage command and the trigger signal in the feedback control mechanism. $C_1$, $D_1$, and $D_2$ denote a clamped capacitor, a clamped diode, and a rectifier diode in the passive regenerative

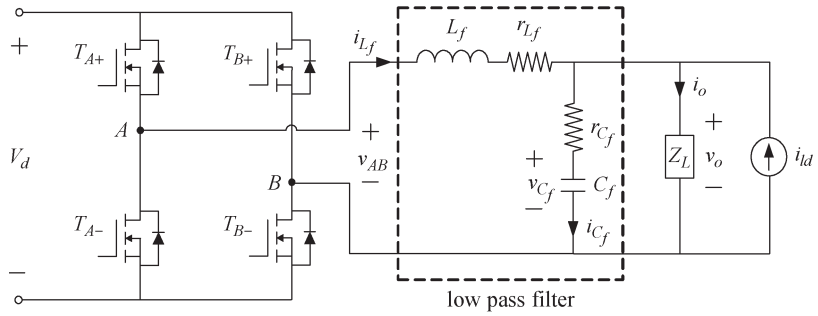


Fig. 3. PWM inverter framework.

snubber circuit. $C_2$ is a high-voltage capacitor in the secondary-side circuit. $D_{\rm o}$ and $C_{\rm o}$ are the output diode and the filter capacitor in the filter circuit. $V_{\rm d}$ and $I_{\rm d}$ describe dc output voltage and current in the dc output circuit.

The coupled inductor in Fig. 2 could be modeled as an ideal transformer, a magnetizing inductor $(L_{\rm m})$, and a leakage inductor $(L_{\rm k})$. The turns ratio $(n)$ and coupling coefficient $(k)$ of this ideal transformer are defined as

$$n = N_2/N_1 \tag{1}$$

$$k = L_{\rm m}/(L_{\rm k} + L_{\rm m}) \tag{2}$$

where $N_1$ and $N_2$ are the winding turns in the primary and secondary sides, respectively. The voltages across the switch, the primary and secondary winding of the ideal transformer, and the leakage inductor are denoted as $\nu_{\rm DS}$, $\nu_{\rm Lm}$, $\nu_{L2}$, and $\nu_{\rm Lk}$, respectively. Moreover, the primary current $(i_{L1})$ of the coupled inductor is composed of the magnetizing current $(i_{\rm Lm})$ and the primary induced current $(i_1)$. The secondary current $(i_{L2})$ is formed by the primary induced current $(i_1)$ through the ideal transformer, and its value is related to the turns ratio $(n)$. In addition, the conductive voltage drops of the switch $(Q)$ and all diodes ($D_{\rm o}$, $D_1$, and $D_2$) are neglected to simplify circuit analyses.

According to the detailed circuit analyses in [17], the voltage gain $(G_{\rm V})$ of the high step-up converter and the corresponding switch voltage $(\nu_{\rm DS})$ can be represented as

$$G_{\rm V} = \frac{V_{\rm d}}{V_{\rm pv}} = \frac{2+nk}{1-D} + \frac{D(1-k)(n-1)}{1-D} \tag{3}$$

$$\nu_{\rm DS} = \frac{V_{\rm pv}}{1-D} + \frac{D(1-k)(n-1)}{2(1-D)} V_{\rm pv} \tag{4}$$

where $D$ is the duty cycle of the switch $(Q)$. Because the voltage gain $(G_{\rm V})$ is less sensitive to the coupling coefficient $(k)$, (4) and (5) can be rewritten with $k = 1$ as

$$G_{\rm V} = V_{\rm d}/V_{\rm pv} = (2+n)/(1-D) \tag{5}$$

$$\nu_{\rm DS} = V_{\rm pv}/(1-D). \tag{6}$$

According to (5) and (6), one can obtain

$$\nu_{\rm DS} = V_{\rm d}/(n+2). \tag{7}$$

By analyzing (7), the switch voltage $(\nu_{\rm DS})$ is not related to the input power source $(V_{\rm pv})$ and the switch duty cycle $(D)$ if the values of the output voltage $(V_{\rm d})$ and the turns ratio $(n)$ are fixed. Thus, it can ensure that the maximum sustainable voltage of the switch $(Q)$ is constant. As long as the input voltage is not higher than the switch voltage rating, the high step-up converter can be applied well to low-voltage PV power sources even with large voltage variations. Simultaneously, it can decouple and simplify the control design of the PWM inverter.

## IV. PWM Inverter Control

### A. Dynamic Model Description

Fig. 3 illustrates the PWM inverter framework including four power semiconductors and a low-pass filter. In Fig. 3, $r_{L_{\rm f}}$ and $r_{C_{\rm f}}$ are the equivalent series resistors of the inductor $(L_{\rm f})$ and the capacitor $(C_{\rm f})$ in the low-pass filter; $Z_L$ is the output load; $\nu_{AB}$, $\nu_{C_{\rm f}}$, and $\nu_{\rm o}$ are the output voltage of the full-bridge inverter, the voltage across the filter capacitor, and the load voltage, respectively; $i_{L_{\rm f}}$, $i_{C_{\rm f}}$, and $i_{\rm o}$ are the filter inductor current, the filter capacitor current, and the load current, respectively; the current source $i_{ld}$ emulates the disturbance incurred by load variations. For convenient analysis, the following assumptions are made in this PWM inverter framework.

1) The values of $r_{L_{\rm f}}$ and $r_{C_{\rm f}}$ are small enough to be ignored.
2) The conduction and switching losses are zero since all power switches are assumed to be ideal devices.
3) The delay time between the switch turn-on and turn-off states is small enough to be neglected.
4) The control signal and I/O voltages are taken as constant values because the switching frequency is much greater than the system dynamic frequency.

Note that the realistic effects of the corresponding elements in 1)–4) still exist in practical applications. Nevertheless, it can simultaneously verify the powerful robustness of the designed inverter control scheme in practice.

Due to the symmetry property of the positive-half and negative-half period in the unipolar PWM switching, the dynamic equation during the positive-half period can be represented via the state-space average method and the linearization technique [12] as

$$\dot{i}_{L_{\rm f}} = (D_i V_{\rm d} - \nu_{C_{\rm f}})/L_{\rm f} \tag{8}$$

$$\dot{\nu}_{C_{\rm f}} = (i_{L_{\rm f}} + i_{ld} - i_{\rm o})/C_{\rm f} \tag{9}$$

$$\nu_{\rm o} = \nu_{C_{\rm f}} \tag{10}$$

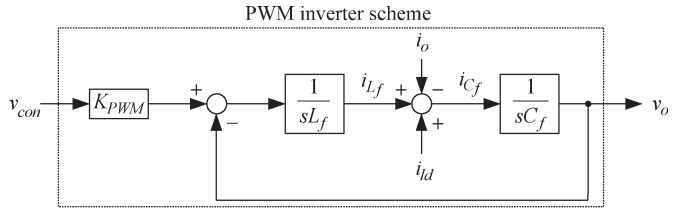


Fig. 4. Equivalent dynamic model of the PWM inverter.

where $D_i$ is the duty cycle of the switches $T_{A+}$ and $T_{B-}$ during one switching period. Define the duty cycle and the power gain as $D_i = \nu_{\rm con}/\hat{\nu}_{\rm tri}$ and $K_{\rm PWM} = V_{\rm d}/\hat{\nu}_{\rm tri}$, where $\nu_{\rm con}$ is a sinusoidal control signal and $\hat{\nu}_{\rm tri}$ is the amplitude of a triangular carrier signal $(\nu_{\rm tri})$, then the dynamic equation of the PWM inverter can be given as

$$\ddot{\nu}_{\rm o} = -\frac{1}{L_{\rm f}C_{\rm f}}\nu_{\rm o} + \frac{K_{\rm PWM}}{L_{\rm f}C_{\rm f}}\nu_{\rm con} - \frac{1}{C_{\rm f}}\dot{i}_{\rm o} + \frac{1}{C_{\rm f}}\dot{i}_{ld}. \tag{11}$$

By way of the Laplace transformation of (11), the equivalent dynamic model of the PWM inverter is depicted in Fig. 4, where $s$ is the Laplace operator.

By choosing the ac output voltage $(\nu_{\rm o})$ as the system state and the control signal $(\nu_{\rm con})$ as the control input, (11) can be rearranged as

$$\begin{aligned}\ddot{x}(t) &= a_p x(t) + b_p u(t) + c_p z(t) + m(t)\\ &= (a_{pn} + \Delta a_{pn})x(t) + (b_{pn} + \Delta b_{pn})u(t)\\ &\quad + (c_{pn} + \Delta c_{pn})z(t) + m(t)\\ &= a_{pn}x(t) + b_{pn}u(t) + c_{pn}z(t) + w(t)\end{aligned} \tag{12}$$

where $x(t) = \nu_{\rm o}$, $u(t) = \nu_{\rm con}$, $a_p = -1/(L_{\rm f}C_{\rm f})$, $b_p = K_{\rm PWM}/(L_{\rm f}C_{\rm f})$, $c_p = -1/C_{\rm f}$, $z(t) = \dot{i}_{\rm o}$ and $m(t) = \dot{i}_{ld}/C_{\rm f}$; $a_{pn}$, $b_{pn}$, and $c_{pn}$ denote the nominal values of $a_p$, $b_p$, and $c_p$, respectively; $\Delta a_{pn}$, $\Delta b_{pn}$, and $\Delta c_{pn}$ represent the system parameter variations; $w(t)$ is called the lumped uncertainty and defined as

$$w(t) = \Delta a_{pn}x(t) + \Delta b_{pn}u(t) + \Delta c_{pn}z(t) + m(t). \tag{13}$$

Here, the bound of the lumped uncertainty is assumed to be given; that is

$$|w(t)| < \rho \tag{14}$$

where $|\cdot|$ is the operator of an absolute value, and $\rho$ is a given positive constant.

### B. ATSMC System

The objective of the PWM inverter control is to force the system state $(x = \nu_{\rm o})$ to track a reference output voltage $(x_{\rm d} = \nu_{\rm cmd})$ under the possible occurrence of system uncertainties. An ATSMC system as shown in Fig. 5 is introduced for the voltage control of the PWM inverter, where the control error is chosen as $e = x - x_{\rm d} = \nu_{\rm o} - \nu_{\rm cmd}$. Define a sliding surface [25] as

$$s_l(t) = c(\boldsymbol{e}) - c(\boldsymbol{e_0}) - \int_0^t \frac{\partial c}{\partial \boldsymbol{e}^{\rm T}}\mathbf{A}\boldsymbol{e}\,d\tau \tag{15}$$

where $\mathbf{e} = [e \quad \dot{e}]^{\rm T}$; $\mathbf{A} = \begin{bmatrix} 0 & 1 \\ -k_2 & -k_1 \end{bmatrix}$, in which $k_1$ and $k_2$ are nonzero positive constants; the function $c$ is designed to satisfy the condition of $\partial c/\partial \boldsymbol{e}^{\rm T} = [0 \quad b_{pn}^{-1}]$; $\boldsymbol{e_0}$ is the initial state of $\boldsymbol{e}(t)$.

The ATSMC system is divided into three main parts. The first part addresses the performance design. The objective is to specify the desired performance in terms of the nominal model, and it is referred to as the baseline model design $(u_{\rm b})$. Following the baseline model design, the second part is the curbing controller design $(u_{\rm c})$ to totally eliminate the unpredictable perturbation effect from the parameter variations and external disturbance so that the baseline model design performance can be assured. Finally, the third part is the adaptive observation design $(\hat{\rho})$ to estimate the upper bound of the lumped uncertainty to alleviate the chattering phenomenon caused by the inappropriate selection of a conservative constant control gain in the curbing controller. The entire control methodologies of the ATSMC system are summarized in the following theorem.

*Theorem 1:* If the PWM inverter scheme shown in (12) is controlled by the three-part ATSMC system described by (16)–(18) with the adaptive observation design shown in (19), then the stability of the ATSMC system for the voltage control of the PWM inverter can be guaranteed

$$u = u_{\rm b} + u_{\rm c} \tag{16}$$

$$u_{\rm b} = -b_{pn}^{-1}(a_{pn}x + c_{pn}z - \ddot{x}_{\rm d} + k_1\dot{e} + k_2 e) \tag{17}$$

$$u_{\rm c} = -\hat{\rho}(t)b_{pn}^{-1}{\rm sgn}\,(s_l(t)) \tag{18}$$

$$\dot{\hat{\rho}}(t) = \frac{1}{\lambda}\,b_{pn}^{-1}\,|s_l(t)| \tag{19}$$

where $\lambda$ is a positive constant.

*Proof:* According to the Lyaponov analyses [22], [23], the stability of the controlled system can be assured. The proof of Theorem 1 is similar to [25] and is omitted here. ■

## V. Active Sun Tracking Scheme

Because the movement of the sun is slow and monotonous, and the variation range of the climbing angle is within $\pm 10^\circ$, it is not necessary to adjust the inclined angle of the PV plate to simplify the mechanical framework. By way of the single-axis direction control, the PV plate can immediately achieve the goal of collecting maximum irradiation. In this paper, an active sun tracking scheme actuated by a synchronous motor is used for the sun tracking via the information of the open-circuit voltage of the PV module. The corresponding control flowchart of the active sun tracker is depicted in Fig. 6.

In Fig. 6, $V_{\rm oc}[n]$ and $V_{\rm oc}[n-1]$ represent the present and previous open-circuit voltages; $\Delta V_{\rm oc}$ denote the variation of

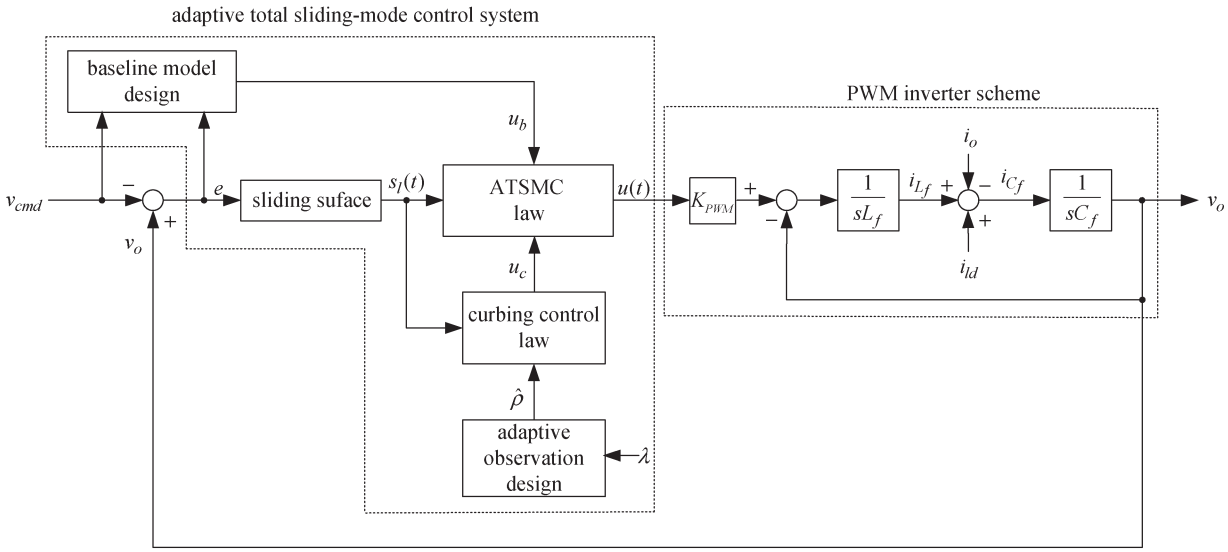


Fig. 5. ATSMC system for the PWM inverter.

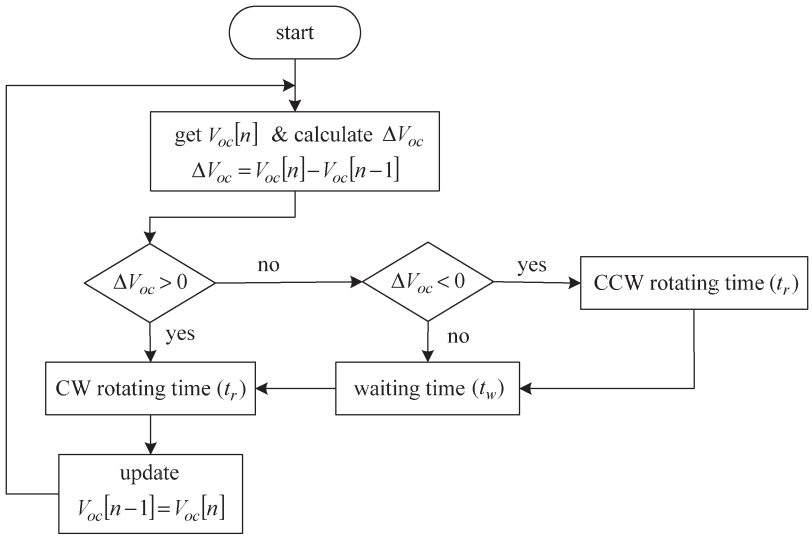


Fig. 6. Control flowchart of the active sun tracker.

the open-circuit voltage. Because the sun only moves from East to West, the PV plate is rotated by the unit angle for time $t_r$ clockwise (CW) in the beginning of the control process to disturb the corresponding open-circuit voltage. This way, it can adjust the rotating direction by observing the variation trend of the open-circuit voltage to capture more irradiation because the open-circuit voltage of the PV module is proportional to the corresponding irradiation. If the condition of $\Delta V_{\rm oc} < 0$ holds, the PV plate is rotated by the unit angle for time $t_{\rm r}$ counterclockwise, i.e., it is returned to the previous location. After that, the control process will wait for time $t_{\rm w}$ to further ensure whether the reason for the decrease of $\Delta V_{\rm oc}$ disappears or not. If the condition of $\Delta V_{\rm oc} = 0$ holds, the control process also waits for time $t_{\rm w}$ for the next CW rotation. Note that the function of the waiting time is helpful for alleviating the extra power consumption in a back-and-forth motion. According to the aforementioned action principle, the control target of the active sun tracking scheme can be achieved.

## VI. Experimental Results

The validity and reliability of the high step-up converter, the PWM inverter control, and the active sun tracker in the high-performance stand-alone PV generation system are verified by the following experimental results.

### *A. Experimental Results of High Step-Up Converter*

To verify the effectiveness of the high step-up converter, the input side consists of six 75-W PV modules manufactured by MOTECH Company (F-MSN-75 W-R-02) connected in parallel as a low-voltage power source. The specifications of a single PV module for the standard condition (1 kW/m$^2$, 25 °C)

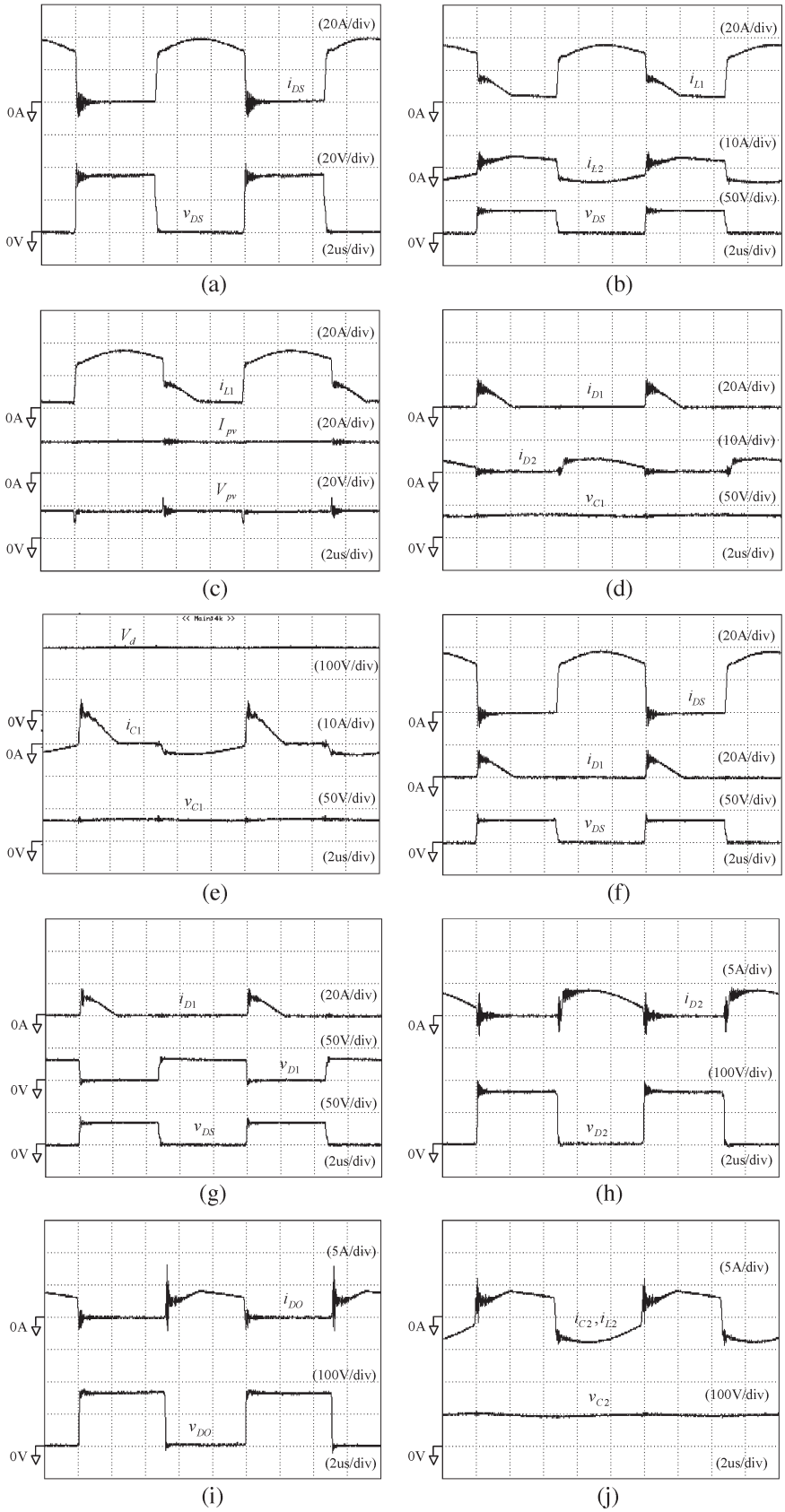


Fig. 7. Experimental voltage and current responses of the high step-up converter with $P_{\rm d} = 320$ W and $V_{\rm d} = 200$ V.

are rated power $= 76.78$ W, rated voltage $= 17.228$ V, rated current $= 4.4567$ A, open-circuit voltage $= 21.61$ V, short-circuit current $= 4.9649$ A, and PV efficiency $= 11.92\%$.

In the experiment, the high step-up converter is designed initially to operate from the variable dc input of PV modules to deliver a constant dc output, $V_{\rm d} = 200$ V. Assume that the

maximum value of the switch voltage is clamped at 34 V, the turns ratio is $n = (V_{\rm d}/\nu_{\rm DS(max)}) - 2 \cong 4$ according to (7). From (6), the related duty cycle, $D \cong 0.7$, is reasonable in practical applications if the minimum input voltage is assumed to be 10 V. To solve the problem of the output voltage of PV modules varied with the load variations, this converter with dc voltage feedback control is utilized to ensure system stability, and a PWM control IC TL494 is adopted to achieve this goal of feedback control. The prototype with the following specifications is designed to illustrate the design procedure given in Section III.

Switching frequency

$$f_{cs} = 100 \text{ kHz}$$

Coupled inductor

$$L_1 = 9\ \mu\text{H} \quad L_2 = 143\ \mu\text{H}$$

$$N_1 : N_2 = 3 : 12 \quad k = 0.97 \quad \text{EE}-55 \text{ core}$$

Capacitor

$$C_{IN} = 3300\ \mu\text{F}/50\ \text{V} * 2$$

$$C_1 = 6.8\ \mu\text{F}/100\ \text{V}$$

$$C_2 = 1\ \mu\text{F}/250\ \text{V} * 2$$

$$C_0 = 680\ \mu\text{F}/450\ \text{V} * 2$$

Switch

$$Q : \text{IRFP2907}\,(75\ \text{V}/209\ \text{A})$$

Diode

$D_1$ : Schottky diode SR2060, TO-220AC$(60\ \text{V}/20\ \text{A})$

$D_2, D_0$ : Schottky diode SB20200CT, TO-220AB

$(200\ \text{V}/20\ \text{A})$.

The experimental voltage and current responses of the high step-up converter operating at 320-W output power $(P_{\rm d})$ are depicted in Fig. 7. From Fig. 7(a), the switch voltage $(\nu_{\rm DS})$ is clamped at 34 V, which is much smaller than the output voltage, $V_{\rm d} = 200$ V, and the curve of the switch current $(i_{\rm DS})$ is similar to a square wave so that it can further reduce the conduction loss of the switch $(Q)$. By observing Fig. 7(b) and (c), the primary current $(i_{L1})$ stays at about 30 A, thus only a smaller core capacity is necessary for $L_1 = 9\ \mu$H. According to Fig. 7(d)–(j), the reverse-recovery currents in all diodes ($D_{\rm o}$, $D_1$, and $D_2$) can be alleviated effectively, and the voltages of the clamped capacitor $(C_1)$ and the high-voltage capacitor $(C_2)$ are close to constant values. Therefore, it can alleviate the reverse-recovery problem and exhibit the voltage-clamped effect to further raise the conversion efficiency. Fig. 8 summarizes the experimental conversion efficiency of the high step-up converter under different output powers. As can be seen from this figure, the conversion efficiency at light powers is over 95% and the maximum efficiency is over 96.5%, which is comparatively higher than conventional converters.

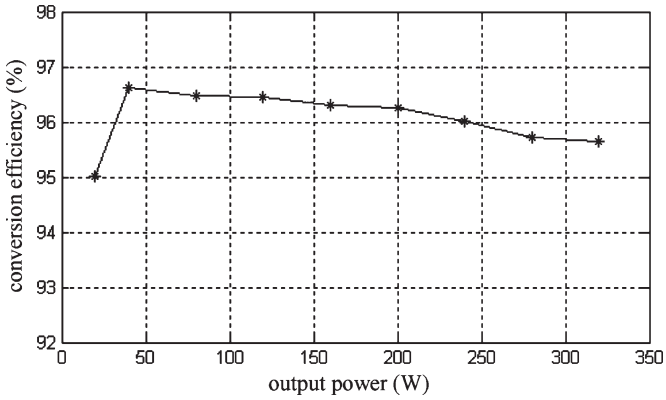


Fig. 8. Conversion efficiency of the high step-up converter with $V_{\rm d} = 200$ V under different output powers.

### *B. Experimental Results of PWM Inverter Control*

The circuit components of the PWM inverter scheme are $(T_{A+}, T_{A-}, T_{B+}, T_{B-})$ IRFP460 (500 V/20 A), $L_{\rm f} = 7.5$ mH, and $C_{\rm f} = 26.8\ \mu$F/250 V; the reference output voltage $(x_{\rm d} = \nu_{\rm cmd})$ is set at ac 110 Vrms, 60 Hz; the switching frequency is $f_{\rm is} = 20$ kHz. Moreover, the parameters of the ATSMC systems for the PWM inverter scheme are given as follows:

$$k_1 = 2.49, \quad k_2 = 830, \quad \lambda = 1.66. \tag{20}$$

All the parameters in the ATSMC system are chosen to achieve the best transient control performance by considering the requirement of stability. For safety consideration, passive or active current limitations should be introduced into the PWM inverter control scheme because only the voltage is controlled in the ATSMC system. In this paper, a passive current limitation mechanism (i.e., a fuse with appropriate current capability) is equipped with the output terminal of the PWM inverter. To exhibit the necessity of the curbing controller, the experimental results of the baseline model control (BSC) in (17) and the ATSMC for the PWM inverter of the high-performance stand-alone PV generation system with fixed resistive load $(R = 100\ \Omega)$ are depicted in Fig. 9. It is obvious that the control performance of the ATSMC system with a lower THD is superior to that of the BSC.

The experimental results of the high-performance stand-alone PV generation system with the ATSMC system for the PWM inverter under step load changes are given to examine the load variation effect. In Fig. 10(a), the resistive load is changed from light load $(R = 300\ \Omega)$ to heavy load $(R = 100\ \Omega)$; reversely, the resistive load is changed from heavy load $(R = 100\ \Omega)$ to light load $(R = 300\ \Omega)$ in Fig. 10(b). As can be seen from this figure, the control performance of the ATSMC system for the PWM inverter is insensitive to the abrupt load changes.

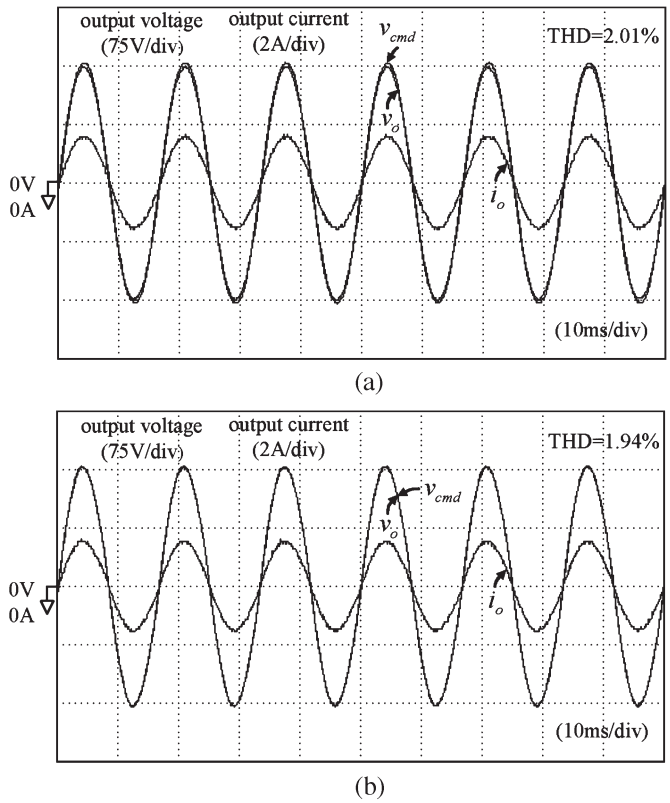


Fig. 9. Experimental results of the high-performance stand-alone PV generation system with fixed resistive load ($R = 100\ \Omega$): (a) BMC for PWM inverter; (b) ATSMC for PWM inverter.

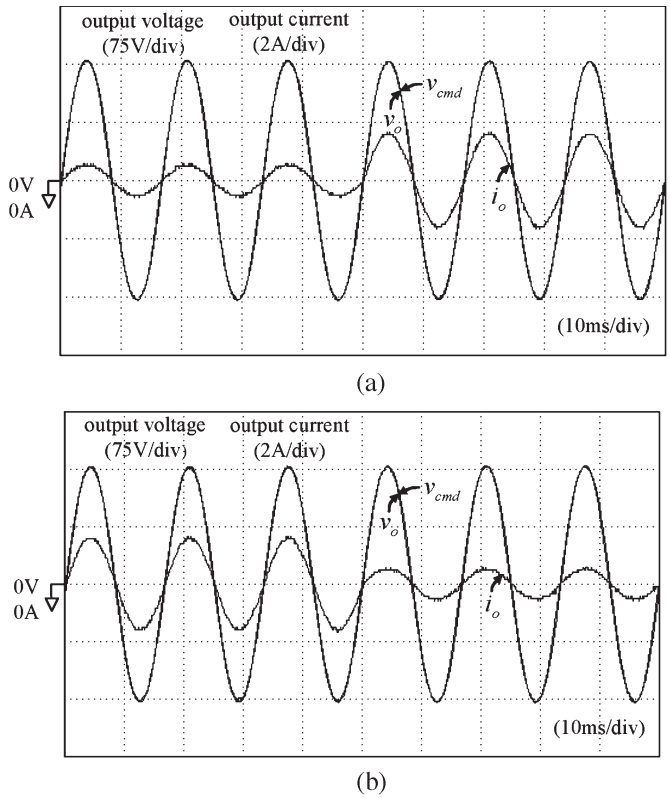


Fig. 10. Experimental results of the high-performance stand-alone PV generation system with ATSMC for PWM inverter under step load changes: (a) Light load ($R = 300\ \Omega$) to heavy load ($R = 100\ \Omega$); (b) Heavy load ($R = 100\ \Omega$) to light load ($R = 300\ \Omega$).

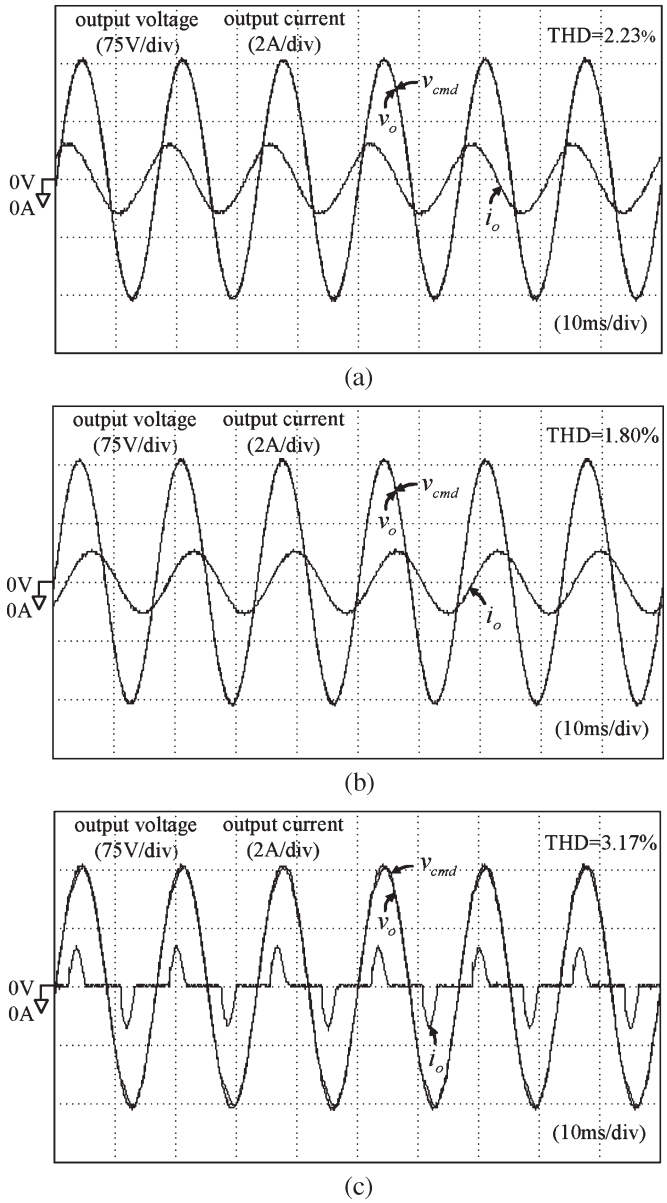


Fig. 11. Experimental results of the high-performance stand-alone PV generation system with ATSMC for the PWM inverter under different load situations: (a) $RC$ load ($R = 100\ \Omega$, $C = 30\ \mu$F); (b) $RL$ load ($R = 100\ \Omega$, $L = 245$ mH); (c) Rectifier with $RC$ load ($R = 500\ \Omega$, $C = 47\ \mu$F).

To further verify the effectiveness of the ATSMC system for the PWM inverter, Fig. 11 illustrates the experimental results under different load situations including an $RC$ load ($R = 100\ \Omega$, $C = 30\ \mu$F), an $RL$ load ($R = 100\ \Omega$, $L = 245$ mH), and a rectifier with $RC$ load ($R = 500\ \Omega$, $C = 47\ \mu$F). By observing Fig. 11, the output voltage ($\nu_{\rm o}$) can almost follow the reference output voltage ($\nu_{\rm cmd}$), and the THD value of the PWM inverter under different loads is less than 5%, which satisfies the demand of the harmonic standards in industrial applications.

### C. Experimental Results of Active Sun Tracker

To verify the validity of the sun tracking scheme by way of realistic experimentations, a single PV module actuated

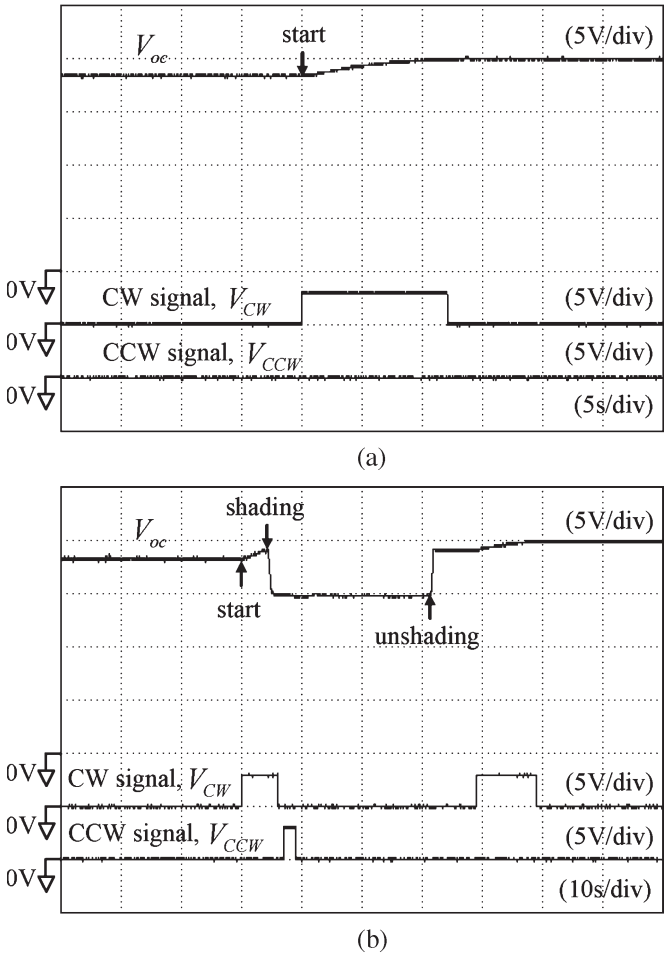


Fig. 12. Experimental results of the high-performance stand-alone PV generation system with active sun tracker: (a) Nominal condition; (b) Shading condition.

by a synchronous motor manufactured by TUSHING Company (GL-301) is used to form the active sun tracker, and the corresponding rotational angle is $3^\circ/\mathrm{s}$. The atmospheric circumstance is the irradiation level of 67 mW/cm$^2$ and the module temperature of 30 °C dated on October 5, 2005 (Local time PM 3:00, Taiwan). The control flowchart as shown in Fig. 6 is implemented using a DSP with 1 ms sampling interval, and the parameters of the active sun tracking scheme are given as follows:

$$t_{\mathrm{r}} = 2\ \mathrm{s}, \quad t_{\mathrm{w}} = 30\ \mathrm{s}. \tag{21}$$

Two conditions of irradiation are examined here: one is the nominal condition, and the other is the shading condition by placing a plastic plate abruptly above the PV plate. The experimental results of the high-performance stand-alone PV generation system with the active sun tracker at nominal and shading conditions are depicted in Fig. 12. In Fig. 12(a), the open-circuit voltage is increased from $V_{\mathrm{oc}} = 18.5$ V to $V_{\mathrm{oc}} = 20$ V when the active sun tracker starts to rotate the PV plate so that it will result in the increase of output power. In Fig. 12(b), the open-circuit voltage is suddenly decreased because the shading condition occurs at 34 s such that the PV plate is returned to its previous location to wait for a time. When the shading condition is removed at 62 s, the PV plate is rotated again after the waiting time to track the sun direction so that the open-circuit voltage is increased to a steady state. According to the experimental results in Fig. 12, the expected goal of the active sun tracker can be achieved perfectly, and this simple active sun tracker mechanism could be used as a controller to further provide the adjustable command for PV arrays of a large-scale PV generation system.

## VII. Conclusion

This paper has successfully developed a high-performance stand-alone PV generation system. The effectiveness of the high step-up converter, the PWM inverter control, and the active sun tracker for the PV generation system was verified by realistic experimentations. According to the results, the maximum conversion efficiency of the high step-up converter is over 96.5%, which is comparatively higher than conventional converters. Moreover, the ac output voltage of the PWM inverter can almost maintain a sinusoidal waveform, and the corresponding THD values under different loads are less than 3.2%, which satisfies the demand of the harmonic standards in industrial applications. In addition, the implementation of the active sun tracking scheme on the basis of the open-circuit voltage of PV modules is to improve the generation efficiency of the fixed-installation PV module, and to save the cost of the conventional sun tracker with light sensors. The original contributions of this paper are the novel investigation of an active sun tracking scheme and the new application of a high step-up converter and a PWM inverter with an ATSMC system in a PV generation system. The salient features of the proposed methodologies with high efficiency dc–dc conversion, larger voltage gain, favorable ac power control quality, and maximum irradiation can be well proven by experimental results. Although the developed high-performance PV generation system belongs to a stand-alone application, it can further merge a maximum-power-point-tracking algorithm and modify the voltage-type PWM inverter control into a current-type to form a grid-connected generation framework.

## Acknowledgment

The authors would like to express their gratitude to the Referees and the Associate Editor for their useful comments and suggestions.

## References

[1] S. R. Bull, "Renewable energy today and tomorrow," *Proc. IEEE*, vol. 89, no. 8, pp. 1216–1226, Aug. 2001.

[2] S. Rahman, "Green power: What is it and where can we find it?" *IEEE Power Energy Mag.,* vol. 1, no. 1, pp. 30–37, Jan./Feb. 2003.

[3] J. A. Gow and C. D. Manning, "Photovoltaic converter system suitable for use in small scale stand-alone or grid connected applications," *Proc. Inst. Electr. Eng.—Electr. Power Appl.*, vol. 147, no. 6, pp. 535–543, Nov. 2000.

[4] T. J. Liang, Y. C. Kuo, and J. F. Chen, "Single-stage photovoltaic energy conversion system," *Proc. Inst. Electr. Eng.—Electr. Power Appl.*, vol. 148, no. 4, pp. 339–344, Jul. 2001.

[5] S. Duryea, S. Islam, and W. Lawrance, "A battery management system for stand-alone photovoltaic energy systems," *IEEE Ind. Appl. Mag.*, vol. 7, no. 3, pp. 67–72, May/Jun. 2001.

[6] Y. K. Chen, C. H. Yang, and Y. C. Wu, "Robust fuzzy controlled photovoltaic power inverter with Taguchi method," *IEEE Trans. Energy Convers.*, vol. 38, no. 3, pp. 940–954, Jul. 2002.
[7] F. Valenciaga and P. F. Puleston, "Supervisor control for a stand-alone hybrid generation system using wind and photovoltaic energy," *IEEE Trans. Energy Convers.*, vol. 20, no. 2, pp. 398–405, Jun. 2005.
[8] J. E. Harry and D. W. Hoare, "Electronic power supplies for high-density discharge (HID) lamps," *Eng. Sci. Educ. J.*, vol. 9, no. 5, pp. 203–206, Oct. 2000.
[9] I. Barbi and R. Gules, "Isolated DC–DC converters with high-output voltage for TWTA telecommunication satellite applications," *IEEE Trans. Power Electron.*, vol. 18, no. 4, pp. 975–984, Jul. 2003.
[10] O. Abutbul, A. Gherlitz, Y. Berkovich, and A. Ioinovici, "Step-up switching-mode converter with high voltage gain using a switched-capacitor circuit," *IEEE Trans. Circuits Syst. I, Fundam. Theory Appl.*, vol. 50, no. 8, pp. 1098–1102, Aug. 2003.
[11] K. C. Tseng and J. Liang, "Novel high-efficiency step-up converter," *Proc. Inst. Electr. Eng.—Electr. Power Appl.*, vol. 151, no. 2, pp. 182–190, Mar. 2004.
[12] N. Mohan, T. M. Undeland, and W. P. Robbins, *Power Electronics: Converters, Applications, and Design*. New York: Wiley, 1995.
[13] M. M. Jovanovic and Y. Jang, "A new, soft-switched boost converter with isolated active snubber," *IEEE Trans. Ind. Appl.*, vol. 35, no. 2, pp. 496–502, Mar./Apr. 1999.
[14] C. M. C. Duarte and I. Barbi, "An improved family of ZVS-PWM active-clamping DC-to-DC converters," *IEEE Trans. Power Electron.*, vol. 17, no. 1, pp. 1–7, Jan. 2002.
[15] R. J. Wai, L. W. Liu, and R. Y. Duan, "High-efficiency voltage-clamped DC-DC converter with reduced reverse-recovery current and switch voltage stress," *IEEE Trans. Ind. Electron.*, vol. 53, no. 1, pp. 272–280, Dec. 2006.
[16] R. J. Wai, C. Y. Lin, R. Y. Duan, and Y. R. Chang, "High-efficiency DC–DC converter with high voltage gain and reduced switch stress," *IEEE Trans. Ind. Electron.*, vol. 54, no. 1, pp. 354–364, Feb. 2007.
[17] R. J. Wai and R. Y. Duan, "High step-up converter with coupled-inductor," *IEEE Trans. Power Electron.*, vol. 20, no. 5, pp. 1025–1035, Sep. 2005.
[18] D. C. Lee and G. M. Lee, "Linear control of inverter output voltage in overmodulation," *IEEE Trans. Ind. Electron.*, vol. 44, no. 4, pp. 590–592, Aug. 1997.
[19] B. Bolsens, K. De Brabandere, J. Van den Keybus, J. Driesen, and R. Belmans, "Three-phase observer-based low distortion grid current controller using an LCL output filter," in *Proc. IEEE Conf. Power Electron. Spec. Conf.*, 2005, pp. 1705–1711.
[20] I. S. Kim and M. J. Youn, "Variable-structure observer for solar-array current estimation in a photovoltaic power-generation system," *Proc. Inst. Electr. Eng.—Electr. Power Appl.*, vol. 152, no. 4, pp. 953–959, Jul. 2005.
[21] S. L. Jung and Y. Y. Tzou, "Discrete sliding-mode control of a PWM inverter for sinusoidal output waveform synthesis with optimal sliding curve," *IEEE Trans. Power Electron.*, vol. 11, no. 4, pp. 567–577, Jul. 1996.
[22] J. J. E. Slotine and W. Li, *Applied Nonlinear Control*. Englewood Cliffs, NJ: Prentice-Hall, 1991.
[23] K. J. Astrom and B. Wittenmark, *Adaptive Control*. New York: Addison-Wesley, 1995.
[24] R. J. Wai and C. H. Tu, "Design of total sliding-mode-based genetic algorithm control for hybrid resonant-driven linear piezoelectric ceramic motor," *IEEE Trans. Power Electron.*, vol. 22, no. 2, pp. 563–575, Mar. 2007.
[25] R. J. Wai, "Adaptive sliding-mode control for induction servomotor drive," *Proc. Inst. Electr. Eng.—Electr. Power Appl.*, vol. 147, no. 6, pp. 553–562, Nov. 2000.
[26] C. C. Kung and K. H. Su, "Adaptive fuzzy position control for electrical servodrive via total-sliding-mode technique," *Proc. Inst. Electr. Eng.—Electr. Power Appl.*, vol. 152, no. 6, pp. 1489–1502, Nov. 2005.
[27] A. Konar and A. K. Mandal, "Microprocessor based automatic sun tracker," *Proc. Inst. Electr. Eng.—Sci. Meas. Technol.*, vol. 138, no. 4, pp. 237–241, Jul. 1991.
[28] B. Koyuncu and K. Balasubramanian, "A microprocessor controlled automatic sun tracker," *IEEE Trans. Consum. Electron.*, vol. 37, no. 4, pp. 913–917, Nov. 1991.
[29] A. Ferriere and B. Rivoire, "An instrument for measuring concentrated solar-radiation: A photo-sensor interfaced with an integrating sphere," *Sol. Energy*, vol. 72, no. 3, pp. 187–193, Mar. 2002.
[30] J. D. Garrison, "A program for calculation of solar energy collection by fixed and tracking collectors," *Sol. Energy*, vol. 72, no. 4, pp. 241–255, Oct. 2002.

**Rong-Jong Wai** (M'99–A'00–M'02–SM'05) was born in Tainan, Taiwan, R.O.C., in 1974. He received the B.S. degree in electrical engineering and the Ph.D. degree in electronic engineering from Chung Yuan Christian University, Chung Li, Taiwan, in 1996 and 1999, respectively.

Since 1999, he has been with the Department of Electrical Engineering, Yuan Ze University, Chung Li, where he is currently a Professor. He is also the Director of the Electric Control and System Engineering Laboratory at Yuan Ze University, and the Energy Conversion and Power Conditioning Laboratory at the Fuel Cell Center. He is a chapter-author of *Intelligent Adaptive Control: Industrial Applications in the Applied Computational Intelligence Set* (Boca Raton, FL: CRC Press, 1998) and the coauthor of *Drive and Intelligent Control of Ultrasonic Motor* (Tai-chung, Taiwan: Tsang-Hai, 1999), *Electric Control* (Tai-chung: Tsang-Hai, 2002) and *Fuel Cell: New Generation Energy* (Tai-chung: Tsang-Hai, 2004). He has authored numerous published journal papers in the area of control system applications. His biography was listed in *Who's Who in Science and Engineering* (Marquis Who's Who) in 2004–2007, *Who's Who* (Marquis Who's Who) in 2004–2007, and *Leading Scientists of the World* (International Biographical Centre) in 2005, *Who's Who in Asia* (Marquis Who's Who), *Who's Who of Emerging Leaders* (Marquis Who's Who) in 2006–2007, and *Asia/Pacific Who's Who* (Rifacimento International) in Vol. VII. His research interests include power electronics, motor servodrives, mechatronics, energy technology, and control theory applications.

Dr. Wai received the Excellent Research Award in 2000, and the Wu Ta-You Medal and Young Researcher Award in 2003, from the National Science Council, Taipei, Taiwan. In addition, he was the recipient of the Outstanding Research Award in 2003, from the Yuan Ze University; the Excellent Young Electrical Engineering Award in 2004, from the Chinese Electrical Engineering Society, Beijing, China; the Outstanding Professor Award in 2004, from the Far Eastern Y. Z. Hsu−Science and Technology Memorial Foundation, Taoyuan, Taiwan; the International Professional of the Year Award in 2005, from the International Biographical Centre, Cambridge, U.K., the Young Automatic Control Engineering Award in 2005, from the Chinese Automatic Control Society, Taipei, Taiwan, and the Yuan-Ze Lecture Award in 2007, from the Far Eastern Y. Z. Hsu-Science and Technology Memorial Foundation, R.O.C.

**Wen-Hung Wang** was born in Taichung, Taiwan, R.O.C., in 1981. He received the B.S. and M.S. degrees in electrical engineering from Yuan Ze University, Chung Li, Taiwan, in 2003 and 2006, respectively.

Now, he serves in the Army, Ministry of National Defense, Taipei, Taiwan. His research interests include photovoltaic generation system, power electronics, and adaptive control.

**Chung-You Lin** was born in Ping-tung, Taiwan, R.O.C., in 1980. He received the B.S. degree in electrical engineering from Yuan Ze University, Chung Li, Taiwan, in 2004. He is currently working toward the Ph.D. degree in electrical engineering at the same university.

His research interests include resonant theory, power electronics, and renewable energy.